Environment Canada

Water Science and Technology Directorate

Direction générale des sciences et de la technologie, eau

Environnement Canada

A Semi-analytical model for the simulation of solute transport in a network of fractures having random orientations

By:
K.S. Novakowski & J.D. Bogan

97-113

A SEMI-ANALYTICAL MODEL FOR THE SIMULATION OF SOLUTE TRANSPORT IN A NETWORK OF FRACTURES HAVING RANDOM ORIENTATIONS

By

K.S. NOVAKOWSKI
and
J.D. BOGAN*

NATIONAL WATER RESEARCH INSTITUTE
867 LAKESHORE ROAD, P.O. BOX 5050
BURLINGTON, ONTARIO
CANADA L7R 4A6

for submission to:
JOURNAL OF CONTAMINANT HYDROLOGY
November, 1996

* Formerly with the Civil Engineering Dept., University of New Brunswick

MANAGEMENT PERSPECTIVE

Title: **A SEMI-ANALYTICAL MODEL FOR THE SIMULATION OF SOLUTE TRANSPORT IN A NETWORK OF RANDOM FRACTURES**

Author(s): K. Novakowski and J. Bogan

NWRI Publ. #:

Citation: Submitted to Journal of Contaminant Hydrology

EC Priority/Issue: In Atlantic Canada, northern Ontario, and various parts of British Columbia, contaminant migration in groundwater circulating through fractures in crystalline rock has contaminated many local water supplies. In Atlantic Canada numerous gasoline stations have leaking underground storage tanks which are the source of this contamination. In northern Ontario, the disposal of low-level nuclear waste in these types of environments may pose a threat to local water supplies. Therefore, the issue is related not only toxics in groundwater but also to the Atomic Energy Control Act.

Current Status: The model developed for this study is being refined and undergoing further verification.

Next Steps: Study is complete. Model may be expanded to look at biochemical processes in granitic rock. Model may be marketed. Value estimated at approximately $2K per copy.

ABSTRACT

A semi-analytical model is developed which accounts for solute transport through a multi-dimensional network of fractures having random orientations and sparse distribution. Transport processes including hydrodynamic dispersion, matrix diffusion, retardation, decay and solute transfer at fracture intersections, are considered. The model is derived by application of the Laplace transform to the governing transport equation for each fracture element. The resulting ordinary differential equations are linked using robust descriptions of mass conservation at the fracture intersections. Solute concentrations are determined by numerically inverting the transformed equations in a sequential fashion. The model is verified using a formal mass balance and through comparison to existing solutions for solute transport in porous and fractured media. To illustrate the use of the model, solute transport in a hypothetical network domain was simulated based on fracture conditions measured at a real field setting in a granitic rock.

INTRODUCTION

Simulating the transport of contaminants in sparsely-fractured media such as granites using models developed for porous media (i.e. a continuum approach) can be shown to be only applicable at a very large scale (Bear, 1993). At the scale typical of a contaminant event, definition of the transport in each discrete fracture is required. In some cases, the groundwater flow system at this scale might be predominated by only one or two fracture features (such as one or two faults) and contaminant transport can be simulated using straightforward analytical models which account for solute transport in a single fracture (eg. Tang et al., 1981). In cases where more than one or two fracture features influence the flow system, definition of the fractures is often conducted using stochastic or stochastic-deterministic methods in two dimensions and solute transport solved for the resulting fracture network using particle-tracking methods (Smith and Schwartz, 1984; Cacas et al., 1990; Dverstorp et al., 1992). For simple orthogonal networks, direct solution of the transport equations for both the fractures and the matrix can be undertaken using finite element methods (Sudicky and McLaren, 1992).

A computationally attractive alternative to these methods, for a multidimensional system of linked fracture elements, is the direct solution of the transport equations using analytical elements. In this case, variations of the solution of Tang et al [1981] in semi-analytical form are used in each fracture element and global concentrations are determined by simultaneous or sequential solution of the equation set. This method is less difficult to implement for non-orthogonal networks than finite-element methods (no discretisation required in the matrix) and offers more flexibility than particle-tracking methods in accounting for transport processes such as matrix diffusion, multi-species transport, and biological transformation.

Semi-analytical models for solute transport in a fracture network based on the solution of Tang et al. [1981] have been developed by Rowe and Booker [1989], Mitchell and Sudicky [1991] and Küpper et al. [1995]. Rowe and Booker [1989] developed a model to account for the transport of conservative species limited to a two- or three-dimensional network of regularly spaced fractures. Transport followed only the regular fracture sets aligned in the direction of flow and mass transfer at fracture intersections was not considered. Küpper et al. [1995a] also developed a model for regular fracture arrangements, although mass transfer at fracture intersections was treated explicitly, in this case. To account for mass transfer, Küpper et al. [1995a] discretized the breakthrough curve in time for each element and used this as input to the next element down-gradient. Comparison of the model configured with several linked one-dimensional elements to the Tang et al solution showed that errors accumulate according to the number of mass transfer events and the coarseness of the discretisation. In an unpublished study, Mitchell and Sudicky [1991] used a Laplace transformed version of the Tang et al. solution (neglecting hydrodynamic dispersion) where mass transfer at fracture intersections was conducted using the equivalent to a Dirichlet boundary condition. Verification of the solution was not conducted.

Mixing at fracture intersections presents an additional problem associated with modeling two-dimensional fracture networks. There are a number of possible approaches including 1) assume complete mixing at each intersection, 2) transfer the solute mass according to stream tube routes at each intersection, and 3) assume only partial diffusive exchange between stream tubes (i.e Berkowitz et al., 1994). Küpper et al. [1995a], determined that if it is assumed that only two fractures can intersect at a given point, out of the four possible flow combinations, three are mathematically

equivalent for both stream tube routing and complete mixing conditions.

In this paper, a semi-analytical model is developed in which solute transport in a non-orthogonal fracture network is solved. Linear transport processes such as hydrodynamic dispersion, adsorption, decay, and matrix diffusion are incorporated. The solution method involves derivation of transport equations for each fracture element by application of the Laplace transform. Virtually any transformable source function can be accommodated at any fracture location. Either complete mixing or stream tube routing and a rigorous definition of mass conservation is used at the fracture intersections. The equations are then solved sequentially using a propagation method. The model is verified by conducting a formal mass balance and by comparison to existing analytical solutions for convection-dispersion and matrix diffusion. To illustrate the use of the model, a simulation is undertaken in a sparsely fractured network typical of fractured crystalline rock.

MATHEMATICAL DEVELOPMENT

To derive a solution to solute transport in a fracture network, a fracture element, as depicted in Figure 1, is defined as the portion of a fracture that lies between the points of intersection with other fractures or with a boundary. Thus, the spatial framework of the fracture system is represented by a set of saturated fracture elements connected at nodes within a homogenous and isotropic matrix. Groundwater flow is assumed to be steady and the aperture along each fracture is assumed to be constant, although variable aperture could easily be accommodated following the method of Nordqvist et al. [1992] . The groundwater velocity in each fracture element is determined using the

method described by Rouleau [1984] and Barker [1991] for steady flow conditions

In the following, a similar approach to that described by Barker [1991] for transient groundwater flow in a network, is used to develop the solution for transport. The transport processes considered include advection, hydrodynamic dispersion, matrix diffusion, adsorption on the fracture surfaces and in the porous matrix, and first order decay.

It is assumed that the porosity of the matrix is sufficiently small such that diffusing solute from adjacent fracture elements do not interact. This is clearly an approximation which will lead to an overestimate of the effect of matrix diffusion for some conditions. The approximation will be of most significance for simulations conducted in domains having short fracture elements and long periods of solute input.

Longitudinal dispersion is assumed to be constant and independent for each fracture element. Adsorption is assumed to be completely reversible and to follow a linear isotherm. Degradation follows a first order decay process and occurs in both the matrix and the fracture at the same rate.

Solute Concentration in a Fracture Element

The governing equations are formulated using constant coefficients for each discrete fracture element within a local co-ordinate system as shown in Figure 1. The equations are developed independently for the fracture and for the matrix and then coupled using a continuity condition between the fracture

and the matrix following the method of Tang et al. [1981].

In Cartesian space, the governing equation for solute transport in a fracture element is [adapted from Tang et al., 1981]

$$\frac{\partial c}{\partial t} + \frac{V}{R}\frac{\partial c}{\partial x} - \frac{\partial}{\partial x}\frac{D}{R}\frac{\partial c}{\partial x} + \lambda c - \left.\frac{\theta D'}{bR}\frac{\partial c'}{\partial z}\right|_{z=b} = 0 \qquad (1)$$

where c and c′ are the concentration of solute in the fracture element and the matrix, respectively, D′is the effective diffusion coefficient of the matrix (includes geometric properties of the pore space), D is hydrodynamic dispersion, V is groundwater velocity, λ is the linear decay constant, θ is the porosity of the matrix, R is the retardation factor in the fracture, and b is ½ the fracture aperture (2b/2). The boundary and initial conditions are

$$c(x, 0) = 0 \qquad (2)$$

$$c(\infty, t) = 0 \qquad (3)$$

$$c(0, t) = c_i(t) \qquad (4)$$

where $c_i(t)$ is the unknown inlet concentration. Note that a specified condition is not applied at the outlet boundary, located at x=L. Thus, it is assumed that the presence of the outlet boundary (i.e. a fracture intersection) has no influence on the solute concentration in the immediate vicinity up-gradient from the boundary.

The differential equation for solute transport in the matrix is given as [after Tang et al., 1981]

$$\frac{\partial c'}{\partial t} - \frac{D'}{R'}\frac{\partial^2 c'}{\partial z^2} + \lambda c' = 0 \qquad (5)$$

where R′ is the retardation factor in the matrix. The boundary and initial conditions for equation (5) are

$$c'(x, \infty, t) = 0 \tag{6}$$

$$c'(x, z, 0) = 0 \tag{7}$$

$$c'(x, b, t) = c(x, t) \tag{8}$$

To solve the system of equations (1) - (8), the Laplace transform method is employed. The solution for solute concentration in the fracture element is:

The Laplace transformed concentration in the fracture is given by $\bar{c}(x,p)$, $\bar{c}_i(p)$ is the Laplace

$$\bar{c}(x,p) = \bar{c}_i(p)\, e^{\nu x(1-E(p))} \tag{9}$$

where

$$\nu = \frac{V}{2D} \tag{10}$$

and

$$E(p) = \sqrt{1 + \frac{4D}{V^2}\left(\frac{\theta\sqrt{D'R'(p+\lambda)}}{b} + R(p+\lambda)\right)} \tag{11}$$

The overbar indicates the Laplace transformed dependent variable, $\bar{c}_i(p)$ is the Laplace transform of the inlet concentration, and p is the Laplace variable.

Flux between Fracture Elements

The transfer of mass between fracture elements is determined as a function of concentration at the fracture intersection. To preserve mass balance, it is necessary to include a dispersive flux term in addition to advective flux at the point of intersection. Thus, the equation that governs the mass flux of solute entering a fracture intersection is given by:

$$J(L, t) = Vc(L, t) - D\frac{\partial c}{\partial x}(L, t) \tag{12}$$

where J is the mass flux term ($ML^{-2}T^{-1}$) that will be used in the assembly of equations for each fracture intersection. Substitution of equation (9) into the Laplace transform of (12) results in the final expression for the flux leaving a fracture element

$$\overline{J}(L, p) = \Phi(p)\, V\overline{c}_i(p)\, e^{\nu L(1-E(p))} \tag{13}$$

where

$$\Phi(p) = \frac{1+E(p)}{2} \tag{14}$$

Therefore, the flux exiting any fracture of length L is dependent only on the inlet concentration and the transport properties of that fracture element.

To determine the solute flux entering a given fracture from a fracture intersection, equation (12) is used with the local coordinate of x=0. Thus, the flux entering is given by

$$\overline{J}(0, p) = \Phi(p)\, V\overline{c}_i(p) \tag{15}$$

where $\Phi(p)$ is as given above.

Solute Transport in a Fracture Network

Because the concentration of solute in a given fracture is dependent only on the inlet concentration for that fracture, a simple propagation method can be used to solve for the distribution of solute in the network. The nodes used to initiate the solution are usually those that constitute the most upgradient in the network. It is not necessary for there to be any solute input at these node, as the

method propagates a null solution until solute input is encountered. However, to simplify the formulation for general conditions at fracture intersections, solute input is limited to boundary nodes.

To formulate a complete solution, the mass flux entering and leaving each node must be summed. Both streamtube routing and complete mixing can be accounted for in this formulation. For example, Figure 2 shows the intersection of two fractures with two different flow arrangements. In Figure 2a, contributing fractures and receiving fractures are opposite one another, while in Figure 2b, contributing and receiving fractures are adjacent. The flow arrangements in Figures 2a and 2b can be classified as mixing and non-mixing (stream tube routing), respectively, according to the definitions given by Küpper et al. [1995a].

The nomenclature used in Figure 2 follows that developed by Barker [1991]. The intersection node is given an integer value, *i*, and fracture elements connected to *i* are defined as j_1 through j_4. Any properties possessed by these fracture elements are given the subscript *j*. The fracture elements defined as *in*, are those that supply flow, and the fracture elements defined as *out*, are those that receive flow.

Assuming no storage of solute at nodes, for uniform flux parallel to the fracture walls across a perpendicular cross-section, $2b_jw_j$, it can be shown that the mass balance at node *i* is

$$\sum_{j=in} J_{(EX)j} 2b_j w_j + F_i = \sum_{j=out} J_{(ENT)j} 2b_j w_j \qquad (16)$$

where J_j is the flux to or from a fracture element, *j*, F_i is the nodal mass rate of flow [M/T] imposed

as a source/sink condition at that location (can be any Laplace-transformable function), and w_j is the unit width of the fracture element. The (EX) subscript indicates that the solute is exiting from a fracture element, and the (ENT) subscript indicates that solute is entering a receiving fracture element. Flux at the exit of an individual fracture element is determined from (13) as

$$\bar{J}_{(EX)j} = \Phi_j(p)\, V_j\, \bar{c}_j(L_j, p) \tag{17}$$

where $\bar{c}_j(L_j,p)$ is the concentration in fracture element, *j*, at the outlet end. The concentration, $\bar{c}_j(L_j,p)$ where $\bar{c}_j(L_j,p)$ is the concentration leaving fracture element, *j*. Similarly, flux at the entrance to a fracture element is determined from equation (15) directly as

$$\bar{J}_{(ENT)j} = \Phi_j(p)\, V_j\, \bar{c}_i(p) \tag{18}$$

The intersection shown in Figure 2a illustrates an example of a configuration in which complete where $\bar{c}_i(p)$ is concentration at the node as calculated during the previous step (see below).

For the complete mixing case (ie. Figure 2a), equations (17) and (18) are substituted into equation (16). This implies that all of the unknown concentrations contributed to receiving fracture elements from the node are equal at the inlets. Then $\bar{c}_i(p)$ is the concentration at the node after mixing has occurred (in the case of non-mixing conditions, this represents the mean concentration within the intersection). This allows us to rearrange the terms and to solve for $\bar{c}_i(p)$

$$\bar{c}_i(p) = \frac{\sum_{j=in} \Phi_j(p)\, Q_j\, \bar{c}_j(L_j, p) + \bar{F}_i(p)}{\sum_{j=out} \Phi_j(p)\, Q_j} \tag{19}$$

where Q_j is the volumetric flow rate in the fracture. Thus, for complete mixing, the outflow concentration from the node is given as

$$\bar{c}_j(0, p) = \bar{c}_i(p) \qquad j=\{out\} \tag{20}$$

where $\bar{c}_j(0,p)$ and $\bar{c}_j(L,p)$ are concentrations located near the intersection, after solute concentration has become homogeneous within the fracture element.

For the one configuration (ie. Figure 2b) that requires incomplete mixing (stream tube routing), a different formulation is applied, following the method suggested by Küpper et al. [1995a]. For the example shown in Figure 2b, $Q_{j1} > Q_{j3}$. In general, when determining concentrations at the intersection, the fracture numbering scheme is arranged so as to be consistent with this flow relation (ie. the fractures are renumbered when $Q_{j1} < Q_{j3}$). For the case shown in Figure 2b, the contribution of solute to fracture j_3 is exclusively from fracture j_1, therefore

$$\bar{c}_{j3}(0,p) = \bar{c}_{j1}(L_{j1},p) \tag{21}$$

Equation (21) is substituted into (16) to determine the remaining inlet concentration. To avoid the problem of distributing external solute input at these types of intersections, as aforementioned, external solute input is limited to the boundary. Thus,

$$\bar{c}_{j4}(0,p) = \frac{[\Phi_{j1}(p)\,Q_{j1} - \Phi_{j3}(p)\,Q_{j3}]\,\bar{c}_{j1}(L,p) + \Phi_{j2}(p)\,Q}{\Phi(p)_{j4}Q_{j4}} \tag{22}$$

To provide a comparison to models in which complete mixing is assumed at all fracture intersections, equation (22) can be replaced by equations (19) and (20).

To implement the solution, numerical inversion of the Laplace concentrations is required. This is conducted using the De Hoog et al [1982] algorithm. This algorithm has been evaluated for inversion of similar transport problems by Moench [1992]. The results indicated that Peclet numbers (the ratio of distance over dispersivity) were limited to the range from 220 to 10,000 depending on the

accuracy of the computer. Similar limitations were encountered in the present study, for the network solution. Further discussion of accuracy is provided in the following section.

Verification and Mass Balance

Additional verification of the model was based on a comparison to existing analytical solutions of Ogata and Banks [1961] and Novakowski [1995]. The results show agreement to 4 significant figures using simple network configurations and comparisons to line elements. Further discussion of these verification procedures can be found in Bogan [1996].

The determination of the total mass of solute in the fracture network is necessary in order to determine the accuracy of the numerical inversion scheme and to evaluate the mass- conservative nature of the model. To perform a formal mass balance at a given time, the following relationship must be proven

$$M_{in} = M_{stored} + M_{out} \tag{23}$$

where in the case of a network of fractures, M_{in} is the total mass of solute introduced into the network at system source nodes, M_{stored} is the total mass of solute stored in the fracture network and surrounding porous matrix, and M_{out} is the total mass of solute that exits the network at exit boundary nodes. Exit boundary nodes are defined as those nodes that have no connected fracture elements to receive flow and thus are the points at which solute leaves the network.

For the purpose of performing the mass balance, only solute concentration in the fracture network is evaluated (matrix diffusion is not considered). Therefore, to determine the M_{stored} for the network, the mass stored in the each fracture element is determined by integration and then summed over the network. Because a spatially dependent equation for the concentration in each element has been developed, an integration performed on this equation with respect to volume yields the mass of the solute. It is assumed that concentration is uniform through a lateral section, which allows the equation to be treated as a one-dimensional problem. Therefore, solute mass in a fracture element, $\overline{M}_j(p)$, can be defined in local coordinates as

$$\overline{M}_j(p) = 2b_j w_j \int_0^{l_j} \overline{c}_j(x, p)\, dx \tag{24}$$

The substitution of equation (9) into (23) and performing the integration yields

$$\overline{M}_j(p) = 2b_j w_j \frac{\overline{c}_j(0, p)}{\nu_j(1 - E_j(p))} \left(e^{\nu L_j (1 - E_j(p))} - 1\right) \tag{25}$$

To determine M_{in} and M_{out}, the cumulative mass of solute that has passed through entrance and exit nodes for the network, respectively, is determined. This mass is accumulated to a given time, $M_i(t)$, and may be evaluated by integrating the flux over time as

$$M_i(t) = \int_0^t F_i(t)\, dt \tag{26}$$

If we perform a Laplace transform on this expression, we obtain

$$\overline{M}_i(p) = \frac{\overline{F}_i(p)}{p} \tag{27}$$

Where $\overline{M}_i(p)$ is the Laplace transform of $M_i(t)$. M_{in} is determined by applying (26) directly at all

system source nodes. M_{out} is estimated by applying (26) to all exit boundary nodes, where $\bar{F}_I(p)$ is determined by the addition of the mass rate of flow to the nodes in equation (15).

To evaluate the mass balance, numerical inversion of the Laplace concentration is required.. To evaluate these limitations, several example simulations were conducted using a stochastically generated fracture network. A mass balance was determined (following the procedure described above) to quantify the total error in the solution.

A series of stochastic networks of increasing fracture density were generated. Log variance of aperture was set to 0.1, in order to include a random component to the flow system. The domain was defined with a dimension in the direction of flow of twice that of the width. Boundary conditions were applied using a constant hydraulic head on the left-hand and right-hand sides of the network. A uniform gradient of 0.002 was induced across the network. The upper and lower boundaries were defined as no-flow. The dispersivity for each fracture ranged from 0.001 to 1.0 for individual realizations. Peclet numbers for the domain were calculated based on the mean path length across the domain. Relative error of the mass balance is expressed as

$$Relative\ Error = \left| \frac{\left(M_{out} + M_{stored}\right) - M^*_{in}}{M^*_{in}} \right| \tag{28}$$

where M^*_{in} is the simple addition of the mass of all Dirac inputs and is an exactly accurate figure. The error was determined for ten snapshots in time for each network. The maximum error for each case is shown in Figure 3, for three fracture densities (F.D.). Due to the stochastic nature of the generation process there was some variation in the error readings. The majority of the error was incurred at early

time.

The total error only exceeded the truncation error of the model ($1.0x10^{-6}$) at Peclet numbers of greater than 1000. This is consistent with the observations of Moench [1991], which suggests that the error observed at Pe < 1000 is introduced solely by the inversion scheme. The error increases in a logarithmic fashion at Pe greater than 1000. In addition, the concentration values at the exit nodes begin to show evidence of increasing "noise" in the solution (random over- or under-estimation of the concentration), usually at early times for these Pe. These limitations are generally encountered in the numerical implementation of inverse Laplace transforms at large Peclet numbers. However, it is important to note that error is small for the range of Pe below 1000. This range is more typical of real field conditions.

RESULTS AND DISCUSSION

To illustrate the use of the model, example simulations are conducted to explain theoretical aspects related to matrix diffusion and to study solute transport using a network which closely follows a field setting in crystalline rock. The purpose of these simulations is to demonstrate the efficiency of the model in testing conceptual models for fracture arrangement and for matrix diffusion.

Generation of Fracture Networks

The development of individual realizations of a fracture network is conducted in two steps. First, a stochastically generated network is constructed using a defined set of fracture statistics. The statistics

include the mean and standard deviation of fracture aperture, length and orientation. The fracture statistics may be obtained from field locations. Second, a set of deterministically defined fractures are overlain on the stochastically generated network. These fractures are intended to more closely simulate field conditions where large scale sheeting fractures predominate the flow system such as at shallow depths in crystalline rock.

Generation of the stochastic component of the fracture network follows the method described by Rouleau [1984]. First, length, orientation, and the location of the centre of the fractures are generated. The lengths of the fractures have a truncated exponential distribution [Schwartz et al., 1983]. To produce the exact linear density of fracture traces within the domain, the end-to-end fracture length is determined by multiplying the area of the domain by the fracture density, and the total generated fracture lengths never exceed this value. In the following discussion, two sets of fractures are stochastically generated, the orientations of which are determined from separate mean and variances. Based on the mean and variance, a normal distribution function is used to generate the orientation of the fracture. The placement of the deterministically defined fractures is conducted by locating the end co-ordinates in the desired positions. The aperture of these fractures were set to values considerably larger than the mean apertures of the stochastically generated network.

Intersections with boundaries and between fractures are then determined. The intersections that lie outside the specified domain are eliminated as are those that connect to dead-end fracture elements. The remaining intersections are defined as nodes in the flow path. Fracture elements are then determined, and the aperture of the parent fracture retained. In the final step, nodes are renumbered in order of their y-position. This reduces the bandwidth of the solution for flow by associating the

spatial position with fracture connectivity, so that the difference in node numbers are more likely to be similar in integer value. An example of a stochastically generated network is shown in Figure 4.

The Effect of Sheeting Fractures

Sheeting fractures occur as extension fractures parallel to the ground surface in crystalline rock [Holzhauser, 1989]. These fractures develop after the formation of fracture sets related to tectonism and are often of larger aperture. In a field study, conducted in monzonitic gneiss [Raven, 1986], sheeting fractures were found to predominate the groundwater flow system at shallow depth. Interconnection between these features was controlled by fractures of smaller aperture and more random orientation. Thus, sheeting fractures form conduits for solute migration and increase the heterogeneity of the network. To investigate the effect that these fractures have on solute transport, several simple sheeting fracture arrangements are superimposed on a finer fracture network, and flow and transport are simulated.

A network with the properties shown in Table 1 was combined with deterministically located fractures shown in the inset of Figures 5a and 5b. The aperture of the deterministically placed fractures was set equal to 200 μm, and the matrix was defined as impermeable. A Dirac source was introduced at the point indicated on the left-hand boundary, and monitored at the point indicated on the right-hand boundary. Errors as determined from mass balance calculations were negligible.

Table 1. Network and transport parameters for simulations.

Network parameters and boundary conditions:	
Fracture Density:	2.5 fractures / m
Domain depth:	30 m
Domain length:	100 m
Mean aperture:	100 μm
Log variance:	0.2
Hydraulic Gradient:	0.01
Transport parameters	
Dispersivity:	0.5 m
Matrix Porosity:	<1%
Matrix Tortuosity:	0.1
Diffusion Coefficient:	6.1×10^{-5} m^2/d

Figure 5a illustrates the results for 10 realizations. The shape of the breakthrough curves are uniformly asymmetrical, with significant tailing observed in some. The asymmetry arises due to transport in the finer fractures. The time of peak arrival is dependent on the arrangement of the interconnections in the finer fracture sets. The breakthrough curve for the case in which the sheeting fracture is through-going and directly connects the entrance and exit (not shown) was observed to have a time to peak arrival of 4.0 days and a symmetrical shape. Thus, although rapid transport occurs in the sheeting fractures, the overall rate of migration is limited by the finer fracture sets.

Figure 5b illustrates a similar scenario in which a third sheeting fracture has been added (see inset). The presence of this fracture results in bi-modal distributions of concentration for some realizations. In addition, the time of arrival of the peak concentration, is much advanced relative to that shown in Figure 5a. Thus, the arrangement of the sheeting fractures can have a profound effect on the transport

properties of a domain such as this. To investigate the presence of the bi-modal distribution, Monte Carlo simulations with 50 realizations were conducted. The presence of bi-modal curves was observed at the same frequency. It is surmised, therefore, that the heterogeneity created by the inclusion of the third sheeting fracture resulted in the breakthrough curves becoming more irregular. However, the asymmetry in the horizontal axis and the relative sparseness of the sheeting fractures also contributes to this effect. Denser sheeting fractures will smooth the breakthrough curves while a sparser arrangement of the vertical fractures will increase the irregular shape of the curves.

Matrix Diffusion

Because the present model is based on a semi-analytical solution, concentrations and flux may be accurately determined over several orders of magnitude. This is useful when analyzing a breakthrough curve at late times, particularly when matrix diffusion is present. Tsang [1995] investigated transport processes by simulating transport in a variety of configurations normally used for tracer experiments. Transport was simulated using particle tracking in a randomly generated network. At low concentrations, random noise was observed, making for a difficult interpretation of the transport processes at late times. On the basis of the results of several simulations, Tsang [1995] proposed that concentrations in the tail of breakthrough curves for tracer experiments conducted in radial flow systems should follow a late-time dependence on $t^{-3/2}$. This was observed in the case for both homogeneous and heterogenous fracture networks.

In this study, several simulations were conducted to investigate these effects in a uniform flow field. The network domain and transport parameters are shown in Table 1. These parameters are based on fracture statistics obtained from the Chalk River area near Ottawa, Ontario. The tracer is introduced at a point on a deterministically located fracture along the border (Figure 4). Deterministically located sheeting fractures were not used in these simulations. The progress of the solute is then monitored at the exit boundary of the network (right hand boundary). Figure 6 illustrates the mass rate of exit (g/day) for matrix porosities ranging from 0% to 1%.

An independent test was conducted to determine the relationship between the mass rate of flow across a boundary and the concentration determined at a specific point. The concentration was determined at a point in the center of the boundary, while the mass rate of exit was determined across the entire exit boundary. For 20 realizations, it was observed that the slope of the mass rate of exit and the concentration at late times follow the same -3/2 log-log slope. In addition, both became increasingly coincident at late times, indicating that the fracture geometry has a decreasing influence on breakthrough when matrix diffusion is included, as shown by Tsang [1995].

In Figure 6, calculation of the log-log slopes show a linear relationship with a slope of approximately $t^{-3/2}$ below a mass rate of exit of 2.5×10^{-4} g/day. This is approximately 0.7% to 9% of the peak rate for porosities of 0.1% to 1%, respectively. Thus, the linear slope is observed under conditions of uniform flow in addition to radial flow systems. For this set of simulations, there is a direct relationship between the porosity and the log-intercept, i.e. as the porosity is increased, the linear portion of the curve is shifted towards a later time by an approximately proportional factor. The lesser the porosity,

the more likely that a point of inflection on the log-log breakthrough curve will occur. It can be observed in Figure 6 that there is both negative and positive curvature in breakthrough curves up to a porosity of 0.5%. At a porosity of greater than 0.5%, there is exclusively negative curvature. In addition, the same effect was observed with increased residence times and coefficients of diffusion. The exact relationship between the inflection of the breakthrough curve and the position of the asymptotic $t^{-3/2}$ approach in specific cases could be determined by inverse analysis.

However, when exploring matrix diffusion using tracer experiments, analytical difficulties in identifying the slope in the breakthrough curve could arise. This is because measurement at late times for low concentrations relative to the peak concentration are prone to higher error, and standing water in the borehole will delay the onset of the slope [e.g. Novakowski, 1992]. Therefore, an analysis of the transition zone, before the onset of the slope, for inflection points and an asymptotic trend towards a -3/2 log-log slope would prove more practical. This is possible because the mid-time curve for zero porosity (generally increasing in steepness to a log-log slope of -4 to -7) is recognizably different from the curve with a porous matrix (trending toward a log-log slope of -1.47 to -1.60 as in these cases).

SUMMARY AND CONCLUSIONS

A semi-analytical model is developed in this paper that simulates flow and transport in a network of fractures. The model is developed using Laplace transforms to eliminate the need for time stepping. Solute transfers at fracture intersections are accomplished with streamtube routing or complete mixing, depending on the hydrodynamics of the fracture intersection. The concentration distribution

in the network is determined using a step-wise solution method. The model was shown to be robust and accurate over a wide range of Peclet numbers. To illustrate the use of the model, applications to fracture networks were conducted to obtain a better understanding of matrix diffusion and the effect of sheeting fractures.

The effect of sheeting fractures was simulated using a rudimentary fracture arrangement overlain on a network of smaller aperture fractures. Significant asymmetry in the breakthrough curves was observed. Bi-modal curves were observed for some realizations. The shape of the breakthrough curves was also found to be sensitive to the arrangement of the smaller aperture fractures that interconnect the sheeting fractures. It is surmised that the denser arrangement of sheeting fractures will smooth the breakthrough curves while a sparser arrangement of the interconnecting fractures will increase the irregularity in the shape of the curve.

Several simulations were also conducted using a network of fractures entirely generated by stochastic means. The results show that, in response to a slug input of solute, the tail of a breakthrough curve at late times is characterized by a slope of $t^{-3/2}$ in log-log concentration. This was also observed by Tsang [1995] for radial flow fields and is attributed solely to the influence of matrix diffusion. Unfortunately, the slope of $t^{-3/2}$ is not apparent until late-time and low concentration, thus diagnosis of matrix diffusion is inhibited. However, based on the simulations conducted for this study, inflection points in the breakthrough curves that occur at mid-time and higher concentration may be useful in this regard.

NOTATION

2b	aperture of the fracture element, L.
c	concentration in fracture element*, M/L^3.
c′	concentration in matrix*, M/L^3.
D	hydrodynamic dispersion, L^2/T.
D′	effective diffusion coefficient within matrix, L^2/T.
E	exponential factor for transport processes.
F	mass rate of flow*, M/T.
J	mass flux *, M/L^2T.
L	length of fracture element, L.
M	mass of solute*, M.
p	Laplace transform of time, 1/T.
Q	volumetric flow, L^3/T.
R	retardation factor in fracture element.
R′	retardation factor in matrix.
t	time, T.
V	average linear velocity of groundwater, L/T.
w	unit width of fracture, L.
x	local co-ordinate parallel to the axis of a fracture element, L.
z	local co-ordinate perpendicular to the axis of a fracture element, L.
θ	porosity of rock matrix.
λ	linear decay constant of solute, 1/T.

ν	V/2D, 1/L.
Φ	dimensionless factor for advective flux.

* May be overlined to indicate that the variable was transformed into the Laplace domain.

Subscripts

(EX)	solute is exiting from the fracture element.
(ENT)	solute is entering into the fracture element.
i	property of a node.
j, j1, j2, j3, j4	property of fracture element.
in	solute entering a collection of nodes at a given time.
out	solute exiting a collection of nodes at a given time.
stored	solute stored in the network. at a given time
n	upper limit of a summation.

ACKNOWLEDGEMENTS

Discussions with Dale Bray, Andrew Piggott, and Ed Sudicky were helpful in developing this model. Funding for this research was provided by Environment Canada.

REFERENCES

Andersson, J. and R. Thunvik, Predicting mass transport in discrete fracture networks with the aid of geometric field data, *Water Resources Research*, 22(13), 1941-1950, 1986.

Barker, J.A., Laplace transform solutions for solute transport in fissured aquifers, *Advances in Water Resources*, 5(2), 98-104, 1982.

Barker, J.A., Reciprocity principle and an analytical solution for Darcian flow in a network, *Water Resources Research*, 27(5), 743-746, 1991.

Bear, J., *Dynamics of Fluids in Porous Media*, Elsevier Science, New York, 1972.

Bear, J., *Hydraulics of Groundwater*, McGraw-Hill, New York, 1979.

Berkowitz, B., C. Naumann, and L. Smith, Mass transfer at fracture intersections: an evaluation of mixing models, *Water Resour. Res,* 30(6): 1765-1773, 1994.

Bogan, J.D., A semi-analytical model for the simulation of solute transport in network of fractures, M.Sc.E Thesis, University of New Brunswick, 92 pp., 1996.

Cacas, M.C., E. Ledoux, G. de Marsily, B. Tillie, A. Barbareau, P. Calmels,

B. Gaillard, and R. Margritta, Modelling fracture flow with a stochastic discrete fracture network:

calibration and validation 2.The transport model, *Water Resources Research*, 26(3), 479-489, 1990.

De Hoog, F.R., J.H. Knight, and A.N. Stokes, An improved method for numerical inversion of Laplace transforms, *SIAM Journal of Science and Statistical Computing*, 3(3), 357-366, 1982.

Dverstorp, B., J. Andersson, and W. Nordqvist, Discrete fracture network interpretation of field tracer migration in sparsely fractured rock, *Water Resources Research*, 28(9), 2327-2343, 1992.

Fujikawa, Y., and M. Fukui, Adsorptive solute transport in fractured rock: analytical solutions for delta-type source conditions, *Journal of Contaminant Hydrology*, 6(1), 85-102, 1990.

Holzhauser, G.R., Origins of sheet structure, 1. Morphology and boundary conditions, *Engineering Geology*, 27, 225-279, 1989.

Hull, L.C., and K.N. Koslow, Streamline routing through fracture junctions, *Water Resources Research*, 22(12), 1731-1734, 1986.

Hull, L.C., J.D. Miller, and T.M. Clemo, Laboratory and simulation studies of solute transport in fracture networks, *Water Resources Research*, 23(8), 1505-1513, 1987.

Küpper, J.A., F.W. Schwartz, and P.M. Steffler, A comparison of fracture mixing models. 1. A

transfer approach to mass transport modelling, *Journal of Contaminant Hydrology*, 18(1), 1-32, 1995.

Maloszewski, P. and A. Zuber, Tracer experiments in fractured rocks: matrix diffusion and the validity of models, *Water Resources Research*, 29(8), 2723 -2735, 1993.

Mitchell, D. and E.A. Sudicky, Analytical solution for solute transport in a two-dimensional fracture network, Unpublished report, University of Waterloo, 32pp., 1991.

Moench, A.F., Convergent radial dispersion: a note on evaluation of the Laplace transform solution, *Water Resources Research*, 27(12), 3261-3264, 1991.

Moreno, L., Y.W. Tsang, C.F. Tsang, F.V. Hale, and I. Neretnieks, Flow and tracer transport in a single fracture: A stochastic model and its relation to some field observations, *Water Resources Research*, 24(12), 2033-2048, 1988.

Novakowski, K.S., An evaluation of boundary conditions for one-dimensional solute transport, *Water Resources Research*, 28(9), 2399-2410, 1992.

Novakowski, K.S., Unpublished notes - solution to continuous input to fracture, 1995.

Ogata, A. and R.B. Banks, A solution for the differential equation of longitudinal dispersion in porous media, *U.S. Geologic Survey Professional Paper 411-A*, 1961.

Raven, K.G., Hydraulic characterization of a small ground-water flow system in fractured monzonitic gneiss, *National Hydrology Research Institute Paper 30*, Ottawa, Ontario, 133 pp, 1986.

Rouleau A., Statistical characterization and numerical simulation of a fracture system: application to groundwater flow in the Stripa granite, Ph.D. Thesis, University of Waterloo, 418 pp., 1984.

Robinson, P.C., Flow and transport in network models of fractured media, Ph.D.Thesis, Oxford University, London, UK, 109 pp, 1984.

Robinson, J.W. and J.E. Gale, A laboratory and numerical investigation of solute transport in discontinuous fracture systems, *Groundwater*, 28(1), 25-36, 1988.

Schwartz, F.W., L. Smith, and A.S. Crowe, A stochastic analysis of macroscopic dispersion in fractured media, *Water Resources Research*, 19(5), p1253-1265, 1983.

Smith, L. and F.W. Schwartz, An analysis of the influence of fracture geometry on mass transport in fractured media, *Water Resources Research*, 20(9), 1241-1252, 1984.

Sudicky, E.A., and E.O. Frind, Contaminant transport in fractured porous media: Analytical Solutions for a System of Parallel Fractures, *Water Resources Research*, 18(6), 1634-1642, 1982.

Sudicky, E.A. and R.G. McLaren, The Laplace transform Galerkin technique for large-scale simulation of mass transport in discretely fractured porous formations, *Water Resources Research*, 28(2), 499-514, 1992.

Tang, D.H., E.O. Frind, and E.A. Sudicky, Contaminant transport in fractured porous media: analytical solution for a single fracture, *Water Resources Research*, 17(3), 555-564, 1981.

Tsang, Y.W., Study of alternative tracer tests in characterizing transport in fractured rocks, *Geophysical Research Letters*, 22(11), 1421-1424, 1995.

Wels, C. and L. Smith, Retardation of sorbing solutes in fractured media, *WaterResources Research*, 30(9), 2547-2563, 1994.

FIGURE CAPTIONS

Figure 1. Schematic of a fracture element and surrounding porous matrix.

Figure 2. Examples of streamline routing at fracture intersections. a) Mixing case. Receiving fractures and contributing fractures are opposite one another (discontinuous intersection). b) Non-mixing case. Receiving fractures and contributing fractures are adjacent to one another (continuous intersection). Fracture numbers are arranged such that $Q_{j1} > Q_{j3}$.

Figure 3. Relative errors from simulation conducted in stochastically generated networks.

Figure 4. Example fracture network. Upper and lower boundaries are no-flow, while the left and right boundaries are constant head. Direction of flow is left to right.

Figure 5. Breakthrough curves from simulations conducted in 10 network realizations. The inset diagram indicates the locations of the deterministically placed fractures in relation to the domain. Breakthrough curves are for a) two sheeting fractures, and b) three sheeting fractures.

Figure 6. Log-log linearity in the tail of breakthrough curves in a densely fractured network, due to matrix diffusion. Slopes approach a value of -3/2.

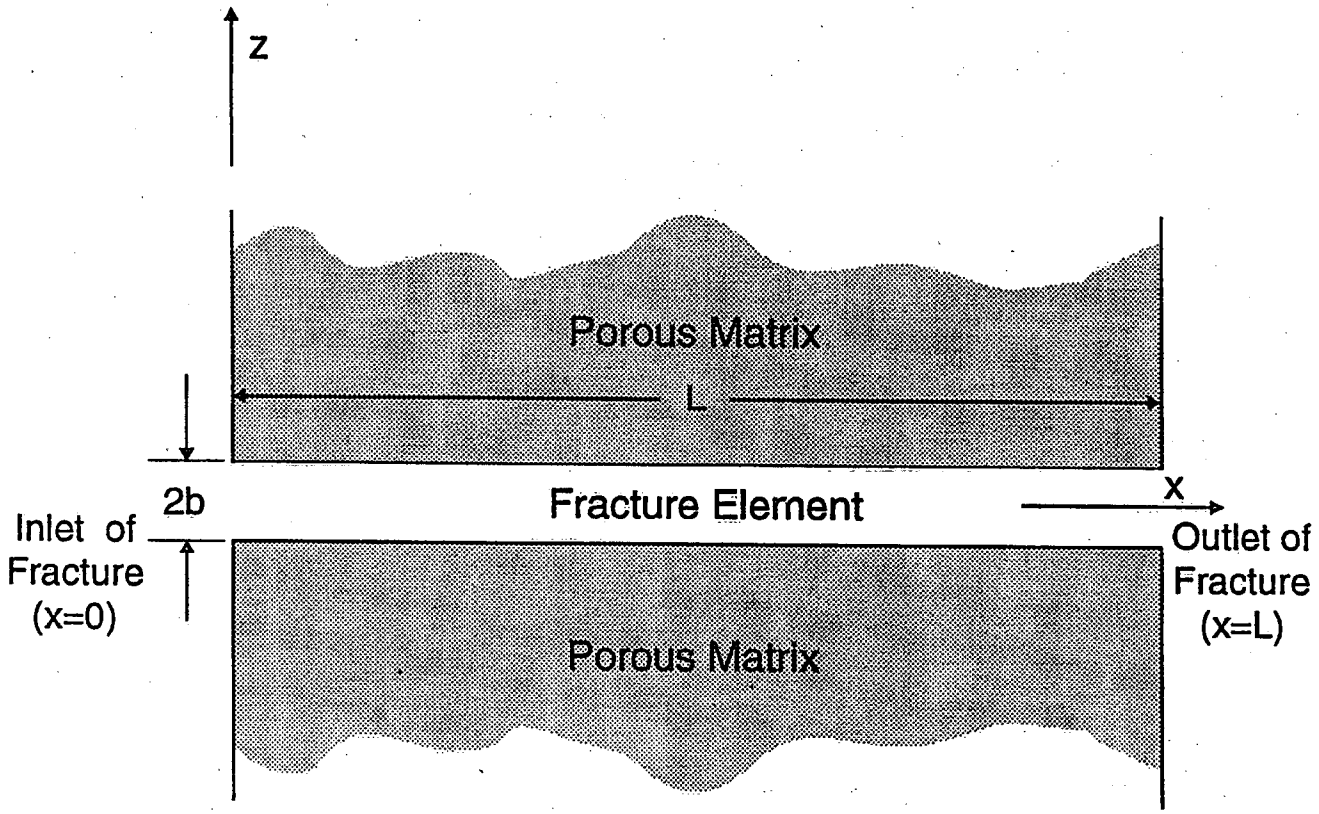

Figure 1. Schematic of a fracture element and surrounding porous matrix.

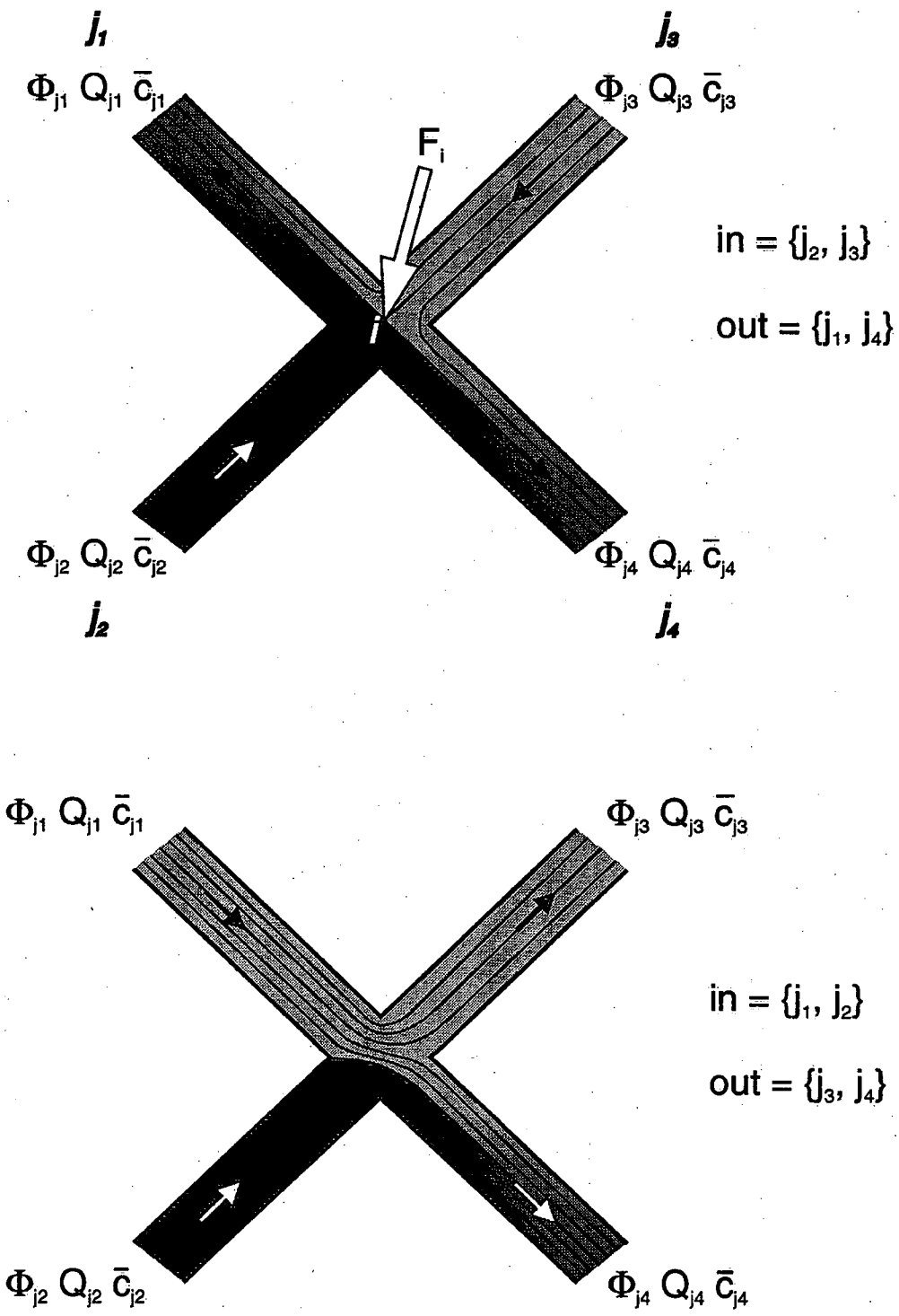

Figure 2. Examples of streamline routing at fracture intersections. a) Mixing case. Receiving fractures and contributing fractures are opposite one another (discontinuous intersection). b) Non-mixing case. Receiving fractures and contributing fractures are adjacent to one another (continuous intersection). Nomenclature is arranged such that $Q_{j3} > Q_{j1}$.

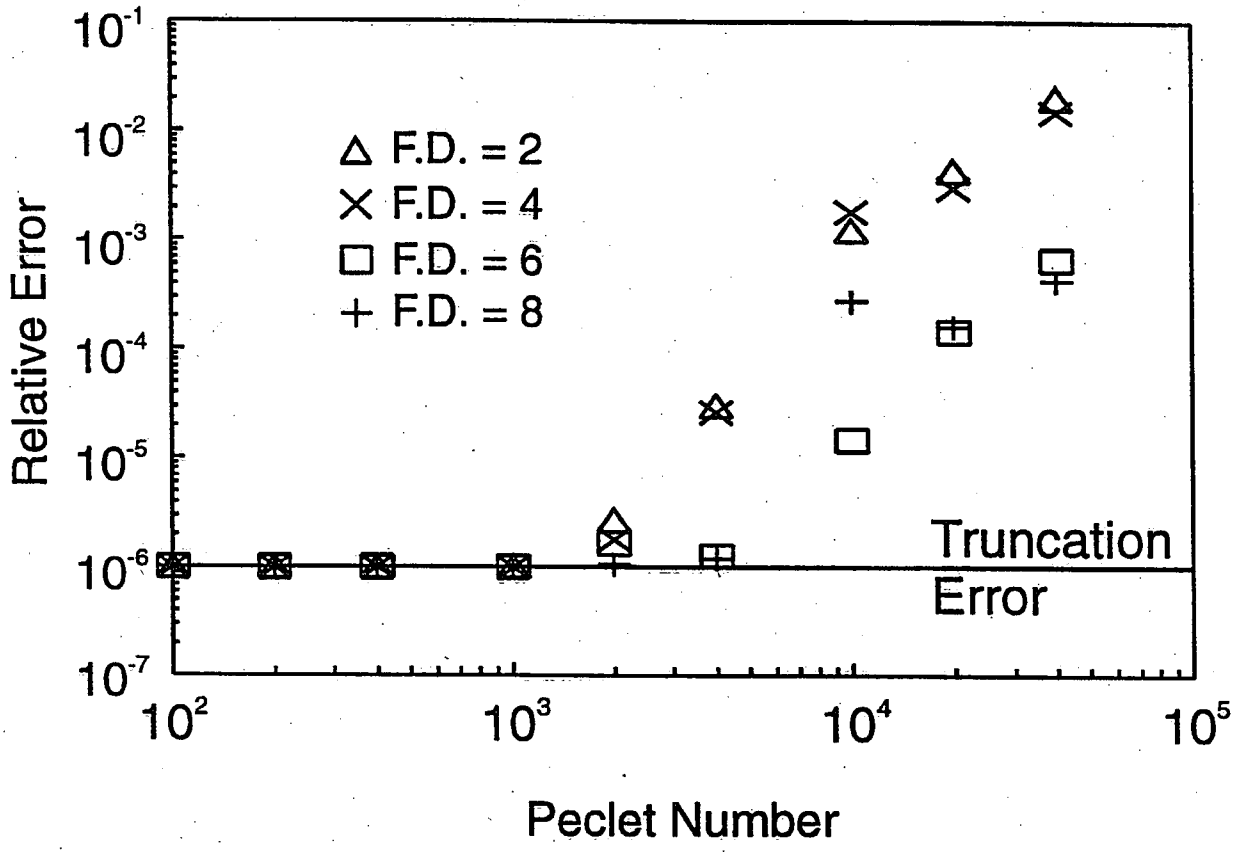

Figure 3. Relative error from simulations conducted in stochastically generated networks.

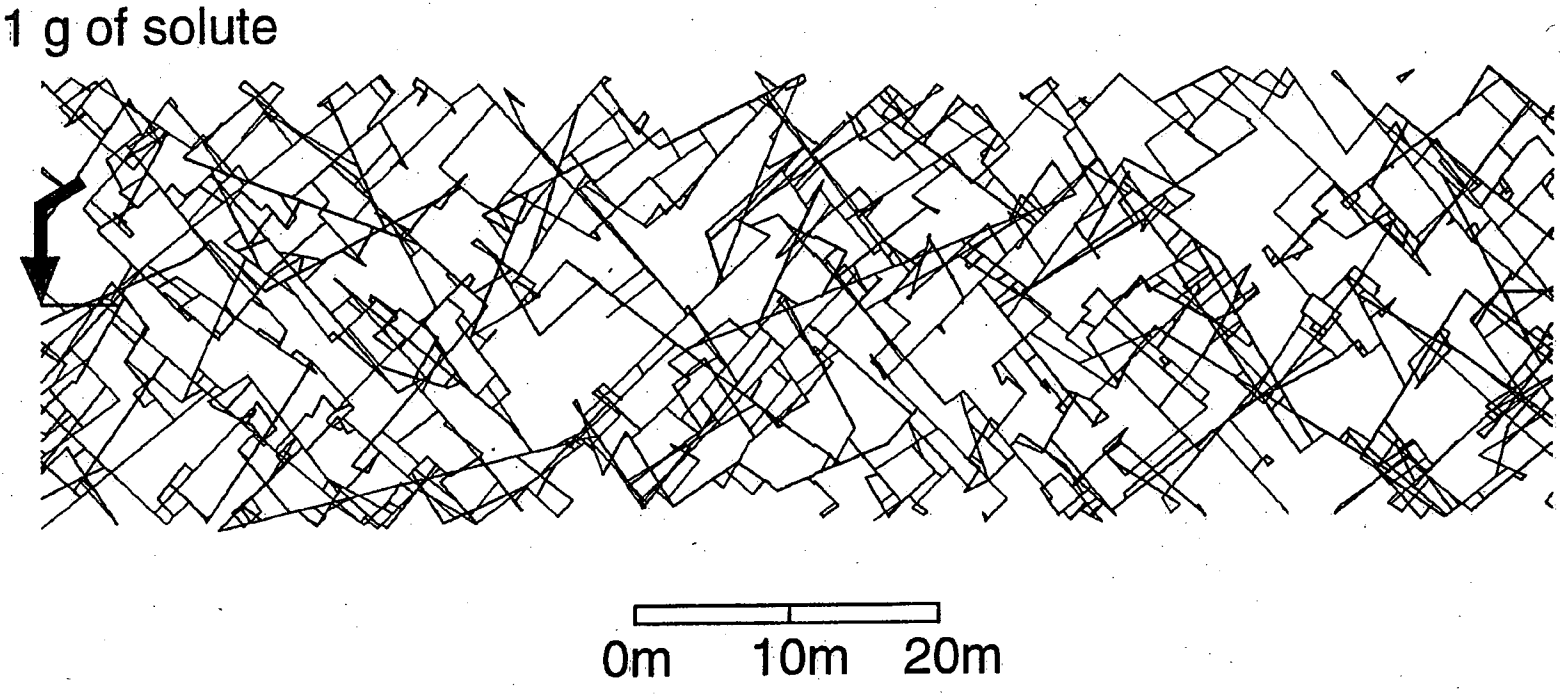

Figure 4. Example fracture network. Upper and lower boundaries are no-flow, while the left and right boundaries are constant head. Direction of flow is left to right.

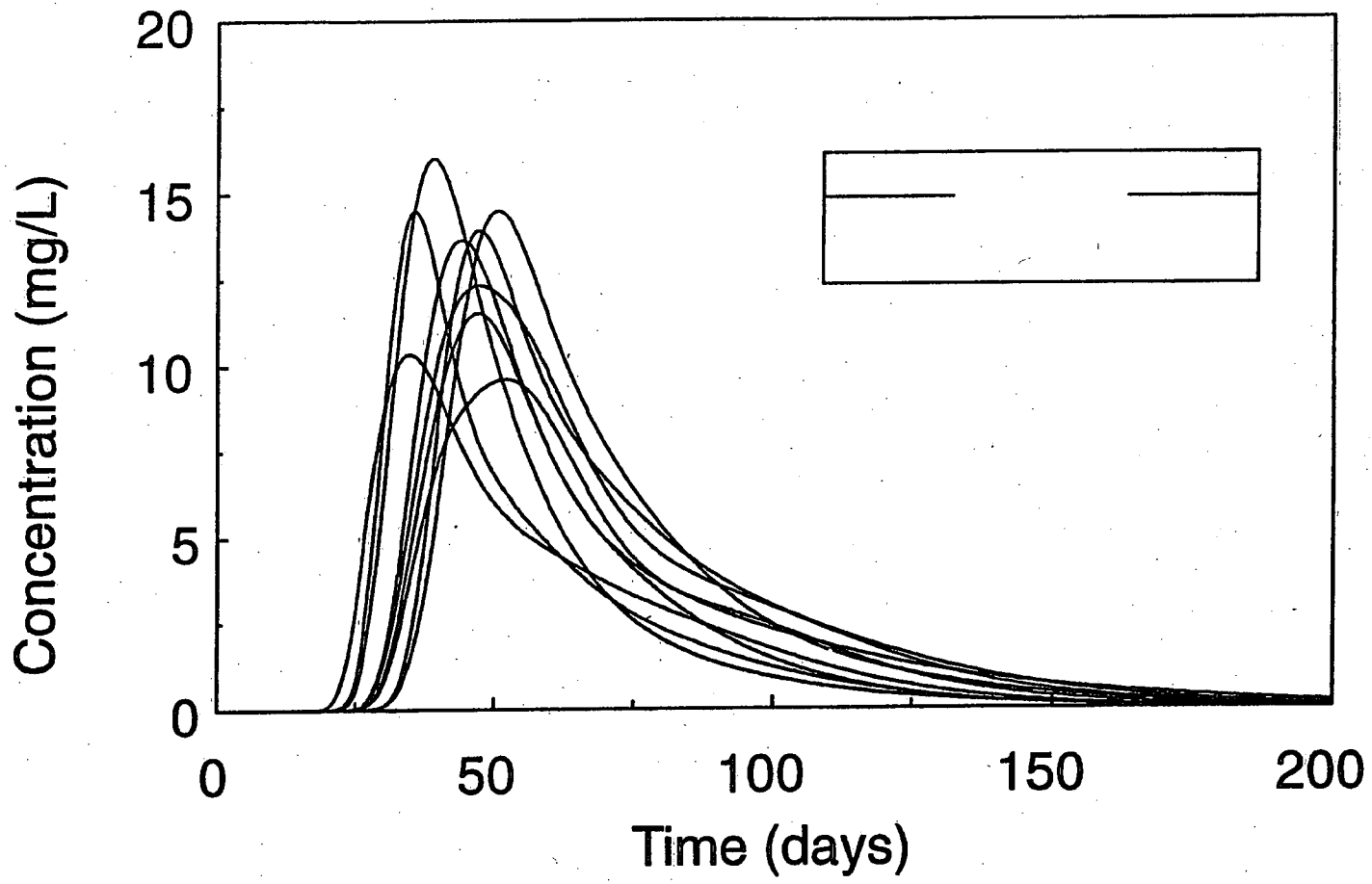

Figure 5. Breakthrough curves from simulations conducted in 10 network realizations. The inset diagram indicates the locations of the deterministically placed fractures in relation to the domain. Breakthrough curves are for a) two sheeting fractures and b) three sheeting fractures.

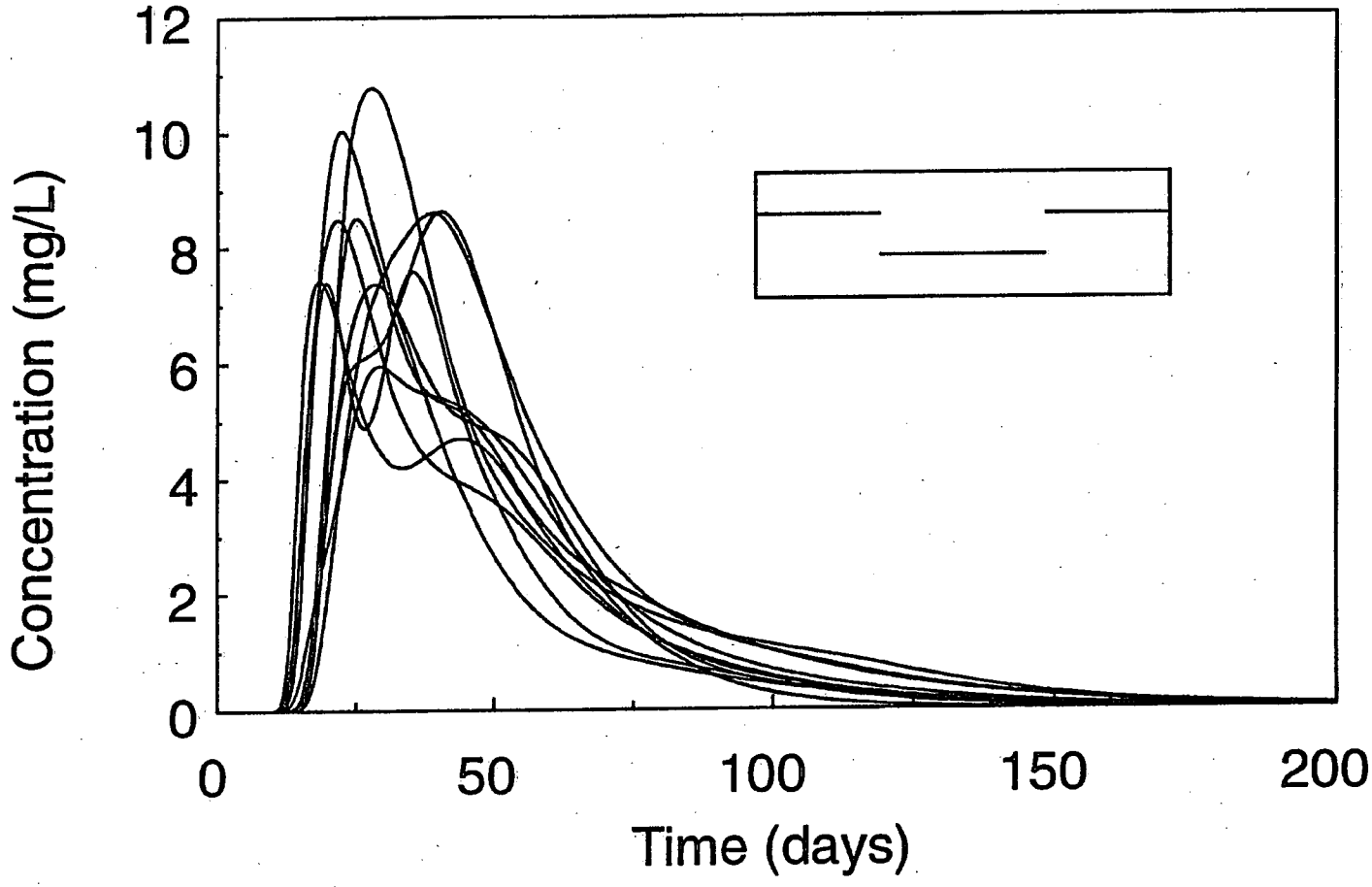
12
10
8
6
4
2
0
Concentration (mg/L)
0
50
100
150
200
Time (days)

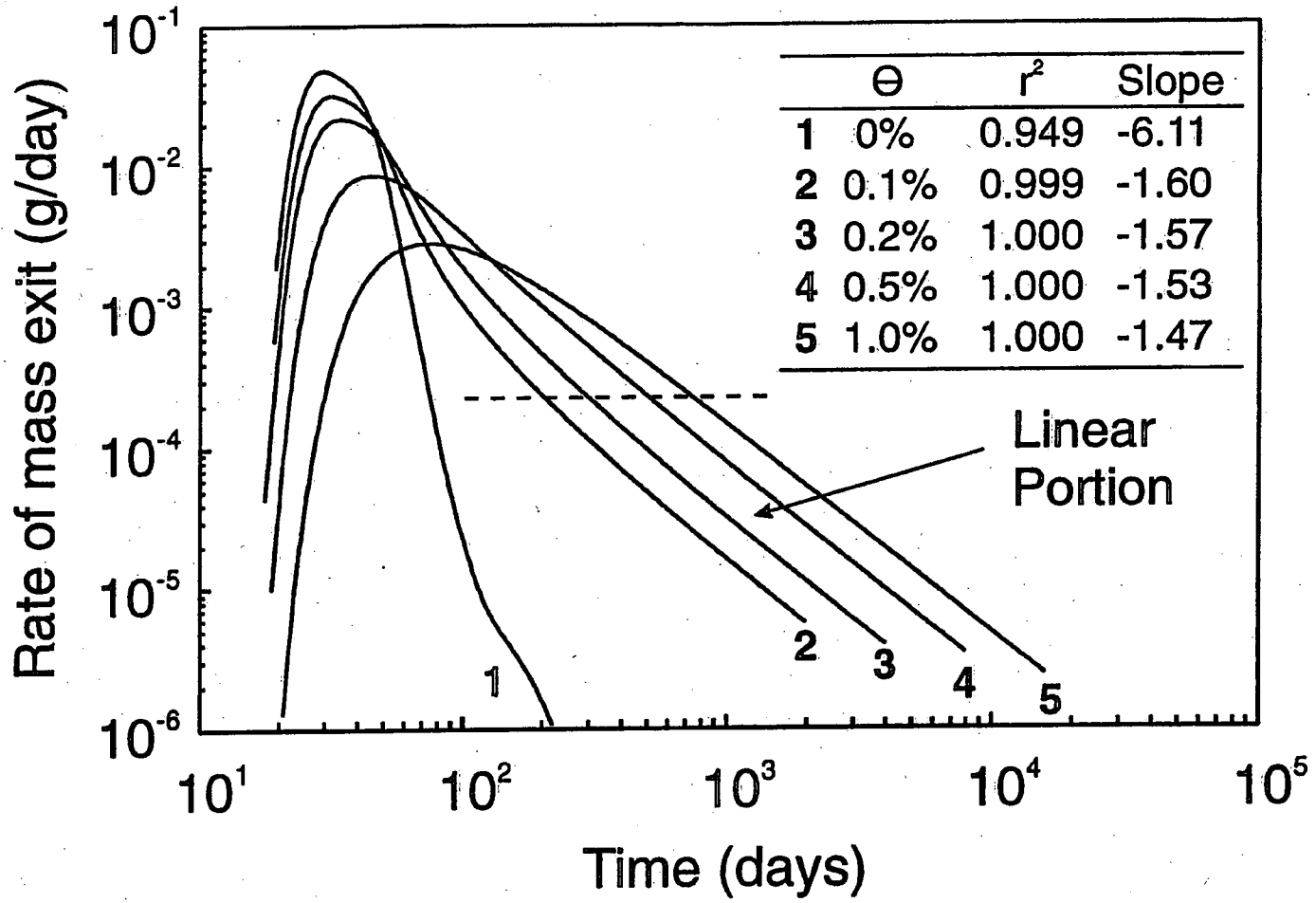

Figure 6. Log-log linearity in the tail of breakthough curves in a densely fractured network, due to matrix diffusion. Slopes approach a value of -3/2.

Environment Canada Environnement Canada

Canada

Canada Centre for Inland Waters
P.O. Box 5050
867 Lakeshore Road
Burlington, Ontario
L7R 4A6 Canada

National Hydrology Research Centre
11 Innovation Boulevard
Saskatoon, Saskatchewan
S7N 3H5 Canada

St. Lawrence Centre
105 McGill Street
Montreal, Quebec
H2Y 2E7 Canada

Place Vincent Massey
351 St. Joseph Boulevard
Gatineau, Quebec
K1A 0H3 Canada

Centre canadien des eaux intérieures
Case postale 5050
867, chemin Lakeshore
Burlington (Ontario)
L7R 4A6 Canada

Centre national de recherche en hydrologie
11, boul. Innovation
Saskatoon (Saskatchewan)
S7N 3H5 Canada

Centre Saint-Laurent
105, rue McGill
Montréal (Québec)
H2Y 2E7 Canada

Place Vincent-Massey
351 boul. St-Joseph
Gatineau (Québec)
K1A 0H3 Canada